Bulletin of the Seismological Society of America, Vol. 98, No. 2, pp. 804–811, April 2008, doi: 10.1785/0120070185

Ⓔ

Short Note

Waveform Relocation and Focal Mechanism Analysis of an Earthquake Swarm in Trichonis Lake, Western Greece

by C. P. Evangelidis, K. I. Konstantinou, N. S. Melis, M. Charalambakis, and G. N. Stavrakakis

Abstract In early April 2007, a series of moderate earthquakes (M_L 4.1–4.8) occurred in the area of Trichonis Lake in western Greece. The earthquake activity was well recorded by the Hellenic Broadband Seismic Network (HL) operated by the National Observatory of Athens. Initial locations for 156 events of the swarm showed a diffuse image of seismicity. Subsequently, 101 events are precisely relocated, calculating source-specific station terms and differential travel times from waveform cross correlation. Uncertainties in relocations are estimated with a bootstrap approach by randomly weighting the original picks and the differential times. Additionally, waveforms of seven out of the eight largest earthquakes of the swarm were inverted in order to derive regional moment tensor solutions. The results showed a tight north-northwest–south-southeast cluster located on an offshore extension of a similarly oriented fault trace mapped onshore. Moment tensor solutions indicate normal faulting with a substantial component of left-lateral strike-slip motion. It is possible that this identified fault forms part of a link that connects the Gulf of Corinth rift system to the west-northwest–east-southeast fault zone south of Trichonis basin.

Online Material: Event catalog and focal mechanism for the eight largest events.

Introduction

On 9 April 2007 at 23:27 (hereafter, all times are given in Greenwich Mean Time) a moderate earthquake with magnitude M_L 4.1 occurred in western Greece and was located at the eastern side of Trichonis Lake. Seismic activity continued with numerous smaller events, and the following day, five larger earthquakes with magnitude M_L 4.8–4.2 followed, respectively. Another event with similar magnitude occurred on 15 April 2007 at 02:14 with M_L 4.0. During this six-day period (9–15 April 2007), 156 events with magnitude $M_L > 3.0$ were identified by the routine analysis of the National Observatory of Athens, Institute of Geodynamics (NOA-IG). The eight largest earthquakes were felt in the broader region of western Greece, but the reported damage to buildings was mainly limited to northeast of the lake, at the village of Thermo (Fig. 1c), where 80 houses and the local high school were partially damaged. Landslides and rockfalls were reported on a road to the northeast of Thermo. Seismic activity resumed again on 5 June 2007 at 11:50 with a similar magnitude earthquake (M_L 4.6).

Trichonis is the largest natural lake in Greece, covering an area of 97 km^2 and located in the western part of the country (Fig. 1a). The lake is particularly important for the people living around it, as it is used as a freshwater source for irrigation and domestic consumption, while its natural beauty attracts a large number of visitors every year. The broader Trichonis basin is a 30-km-long by 10-km-wide neotectonic graben. Its southern border is marked by a major west-northwest trending normal fault (Fig. 1c) that is hidden by Pleistocene deposits and thick alluvial cones (Doutsos *et al.*, 1987). Although there is not direct association of this fault with large modern or historical earthquakes, Goldsworthy *et al.* (2002) have reported evidence of its relative youth that can be seen in the geomorphology and the drainage system of the area. These authors suggest that the north-dipping fault continues to the west on the south side of Lake Lesimachia (Fig. 1c). The Trichonis basin and its associated faults were considered the northwestward extension of a 120° N broader rift zone (Brooks *et al.*, 1988; Melis *et al.* 1989; Melis *et al.*, 1995), centered at the Corinth Gulf where Peloponnese drifts away from mainland Greece (Fig. 1a).

Western Greece is dominated by west-northwest and northeast-trending normal faults and basins that have been formed since late Miocene, due to the back-arc extension of the Hellenic arc and movements transmitted to the Aegean area from the north Anatolian transform fault (Brooks *et al.*, 1988; Doutsos and Kokkalas, 2001; Goldsworthy *et al.*,

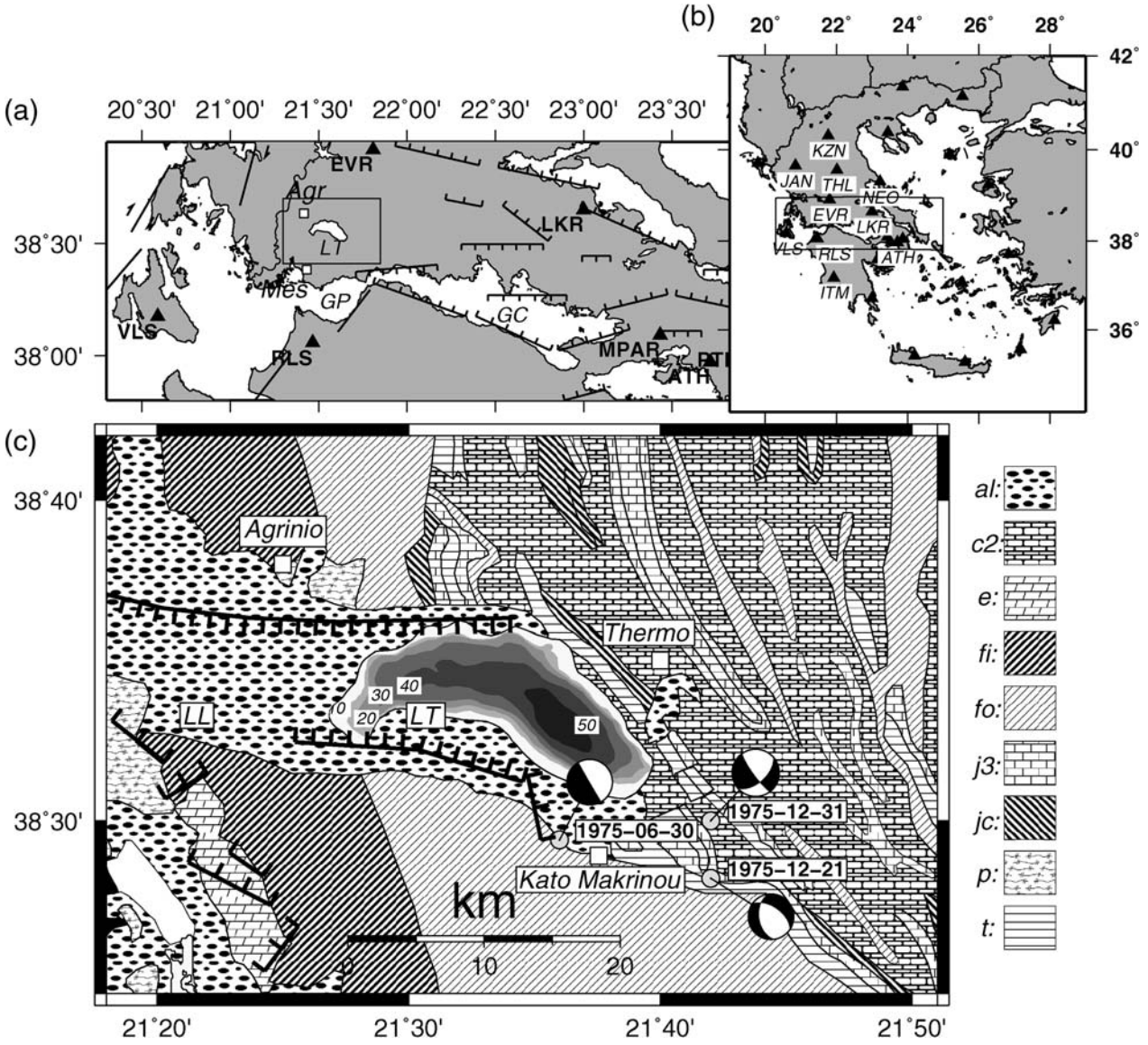

Figure 1. (a) General map of central Greece with faults after Papazachos and Papazachou (1997). Stations of the Hellenic Broadband Seismic Network (HL) are also indicated as black triangles. Rectangle marks the position of map (c). (b) Inset map of the Hellenic peninsula and the Aegean Sea shows the selected area of (a) as rectangle and the NOA-IG, GEOFON, and MedNet stations marked as triangles. These stations used for the waveform relocation (WCC) are indicated with their names. (c) Geological map of the study area with bathymetry of the Trichonis Lake and mapped faults by the Greek Institute of Geology and Mineral Exploration (IGME). Focal mechanism and dates of past events are also plotted. Nearby towns and villages mostly affected by the Trichonis Lake swarm are indicated. Trichonis Lake, LT; Lake Lesimachia, LL; Gulf of Corinth, GC; Gulf of Patra, GP; Agrinio, Agr; Mesolongi, Mes; alluvium, al; upper Cretaceous limestones, c2; Paleocene limestones, e; semimetamorphised flysch, fi; flysch, fo; upper Jurassic limestones, j3; Pindus flysch, jc; Pliocene lacustrine sediments, p; Pyrite slates and limestones, t.

2002). Preexisting north-northwest and east-northeast normal faults and basins were developed, since middle Miocene, parallel and perpendicular to the main thrusting and folding of the Hellenides (Doutsos *et al.*, 1987). As the back-arc stress regime migrated westwards these structures became inactive, however, these older normal faults may be reactivated with a strike-slip character by the applied north–south extensional regime.

As the first analog seismic network in Greece only started operating after 1965, very little is known about the seismicity around Trichonis before that period. Since then, important seismic swarm activity in the area was reported during June and December 1975 (NOA-IG, 1975). The first of the largest events took place on 30 June 1975 at 13:26 with $M_S 5.4/M_L 5.4$ and again on 21 December 1975 at 16:07 with magnitude $M_S 5.8/M_L 5.1$ followed by another event on 31 December 1975 at 09:45 with magnitude $M_S 5.9/M_L 5.1$. Although there are discrepancies in the magnitudes reported in the bulletins for these three events, it appears that the most damaging was the third one with one casualty, 200 houses

destroyed, and 580 houses seriously damaged at the village Kato Makrinou, while the first one had no casualties but caused serious damage to 60 houses. Focal mechanism solutions for these three largest events were derived by Drakopoulos and Delibasis (1982) using first-motion polarities (Fig. 1c). Although all three mechanisms indicate a northwest–southeast fault strike, the sense of motion is different for each of the solutions. It has to be emphasized that the accuracy is low because only polarities from analogue records are used.

In this article, we present an analysis of the earthquake swarm that occurred in Trichonis Lake using high-quality regional waveform data recorded by the Hellenic Broadband Seismic Network (HL), which is operated by NOA-IG. Our analysis starts with the location and accurate relocation of swarm events using both catalogue and waveform cross-correlation differential travel times. We also invert the broadband waveforms in order to derive the regional moment tensors for the seven out of the eight largest events of the swarm. Finally, we discuss our results in connection with the surface geology and tectonics around the lake in order to interpret the relationship of this seismic activity with the prevailing deformation pattern in western Greece.

Data and Initial Locations

The NOA-IG Hellenic Broadband Seismic Network consists of 23 broadband, three-component stations (see Fig. 1b and http://bbnet.gein.noa.gr, last accessed February 2008). Additional data from stations in the eastern Mediterranean region (i.e., GEOFON and MedNet networks) are also available in real time, through an implementation of the SeisComP acquisition software (for details, see Melis and Konstantinou (2006)). For 156 events recorded from 9–15 April 2007 and the last one on 5 June 2007, the *P* and *S* phases were repicked manually. The travel time picks were initially used as input to HYPO2000 (Klein, 2002) for event location using a 1D velocity model that stems from the tomographic study of western Greece published by Haslinger *et al.* (1999). Figure 2a shows the distribution of the initial locations that were obtained in this way. The mean horizontal and vertical errors are 1.4 and 3.8 km, respectively, while there are events with much larger errors that increase the deviation (Fig. 2b,c). These first locations show a considerable scatter of the epicenters over the area of the lake and hypocentral depths that vary from less than 5 to more than 20 km, not allowing the delineation of any seismogenic structure.

Earthquake Relocation

The initial earthquake locations that were obtained previously were subsequently used as input to the relocation method. Based on the same 1D velocity model, *P* and *S* travel-time tables are calculated, and the earthquakes are relocated with the shrinking grid-search algorithm (Lin and Shearer, 2005). The events are separated into smaller groups of neighboring events, and station corrections are calculated for each source-station pair. As introduced by Richards-Dinger and Shearer (2000), the source specific station term (SSST) for each source-station pair represents the weighted median of residuals at a given station from *N* nearby events. The number *N* and the maximum allowed distance between them is defined and reduced in iterations. In our case, it starts with 200 nearby events and a maximum cutoff value of 50 km between events and is gradually reduced after 35 iterations to 10 nearby events and maximum cutoff distance of 5 km. Using a station-event cutoff range of 200 km, 152 events are relocated with the SSST method having a 0.24-sec mean root mean square travel-time misfit.

Differential travel times between two closely spaced events recorded in a station can be obtained either from observed and calculated travel times or directly from cross correlation (WCC) of their waveforms. Differential travel times from WCC are used as additional information to the observed ones in order to solve for a new set of adjusted picks by minimizing the misfit to both the original picks and the differential times (Shearer, 1997). This procedure requires a similar-event cluster identification and is termed as cluster analysis (Shearer *et al.*, 2005).

The waveforms for all events are low-pass filtered at 5 Hz, as it is generally found that WCC is more stable at lower frequencies (e.g., Shearer, 1997; Shearer *et al.*, 2005). To avoid ambiguities associated with the P_g/P_n crossover distance, we cross correlate waveforms from stations within a maximum 200-km epicentral distance. The cross-correlation function is computed for all nearby event pairs at each individual station and, specifically, for windows of 3 and 4 sec around the picked arrival time of *P* and *S* phases, respectively. The number of event pairs at different cross-correlation coefficients (CC) is highest for *P* windows at 0.8 and for *S* windows at 0.55 (Fig. 3a). *P* waves correlate better than *S* waves because the latter are combined with less coherent coda from the *P* waves. Most event pairs correlate with CC higher than 0.55 at a minimum of three stations (Fig. 3b) and the stations with most waveform pairs with CC higher than 0.55 are those in proximity of Trichonis Lake (e.g., THL, EVR, VLS, and RLS; see Figs. 3c and 1b).

Closely spaced events with average CC values, for *P* and *S*, higher than 0.6 in at least three stations define an event cluster. The choice of these values is a compromise between the highest relocation precision and the largest possible number of events that can be assigned to every cluster (Shearer *et al.*, 2003). In our case, this choice insures that all events with magnitude greater than 4 are included within the resulting clusters. Any two different clusters with random events may correlate well to each other for only some events. These two clusters will merge into one, if more than a fraction of the possible correlations have a coefficient greater than 0.6. In our case, using lower than 20% fraction values causes collapsing of all distributed events into a single cluster. There-

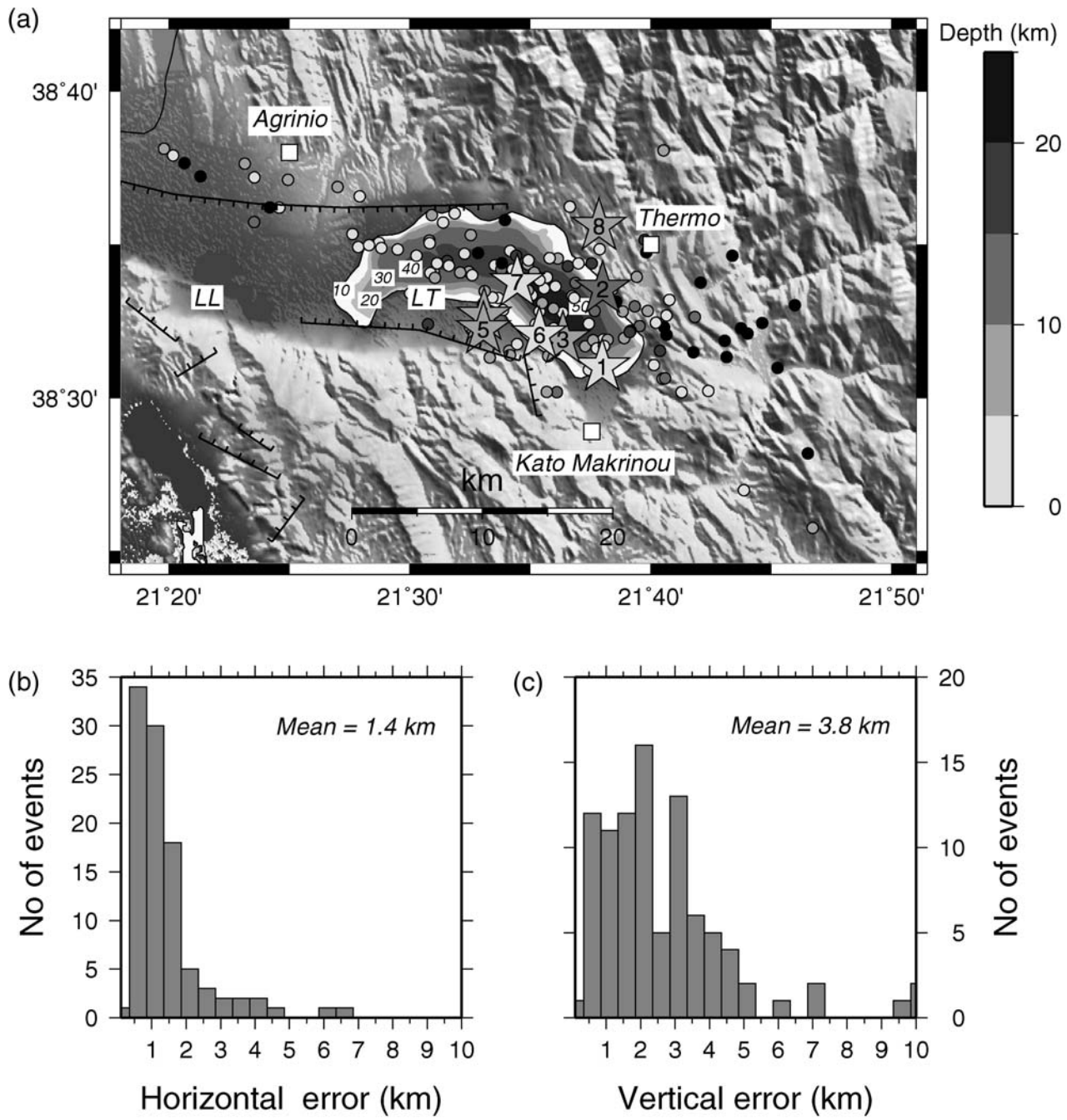

Figure 2. (a) Initially located hypocenters of the Trichonis Lake 2007 swarm are marked as dots in color scale according to hypocentral depth. Numbered stars mark events greater that M_L 4 in chronological order. Lake bathymetry and mapped faults are also marked. (b) and (c) Horizontal and vertical error in kilometers for the events located with HYPO2000. The mean values are also indicated. Note that histograms and mean values are only for the 101 events that were subsequently relocated with SSST and WCC methods, to allow direct comparison with Figure 4.

fore, to ensure that this is not a possible false single cluster, we apply a 20% fraction value to obtain the resulting clusters.

Location uncertainties during WCC relocation are estimated using a bootstrap technique. This method is based on the bootstrap approach by Billings *et al.* (1994) and Shearer (1997) in which random picking errors are added to the travel-time picks, and events are relocated multiple times to account for the location scattering due to uncertainties in the picks. Similarly, a random weighting to the adjusted picks (original picks and differential times) could be applied during their location inversion. This procedure was repeated 200 times in order to obtain a cloud of scattered locations for each event. The standard deviation from each mean event position is a relative error estimate. The mean horizontal and vertical relative uncertainties in our case are found to be 0.9 and 0.6 km, respectively (Fig. 4). A compar-

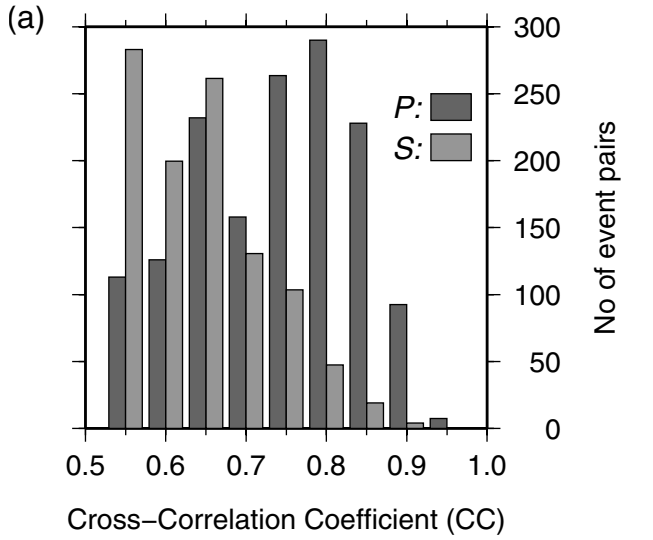

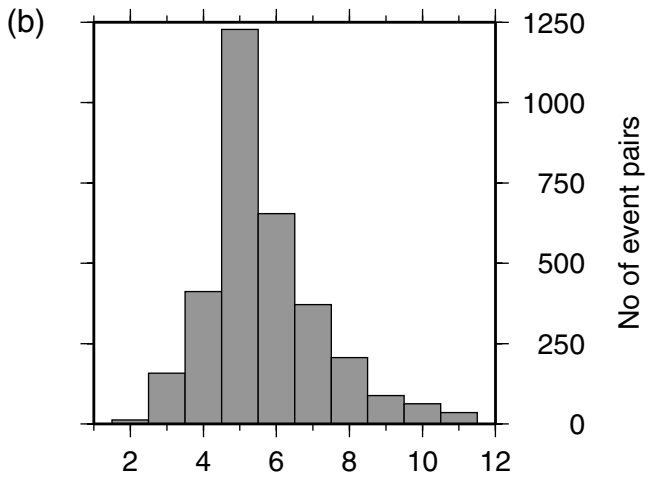

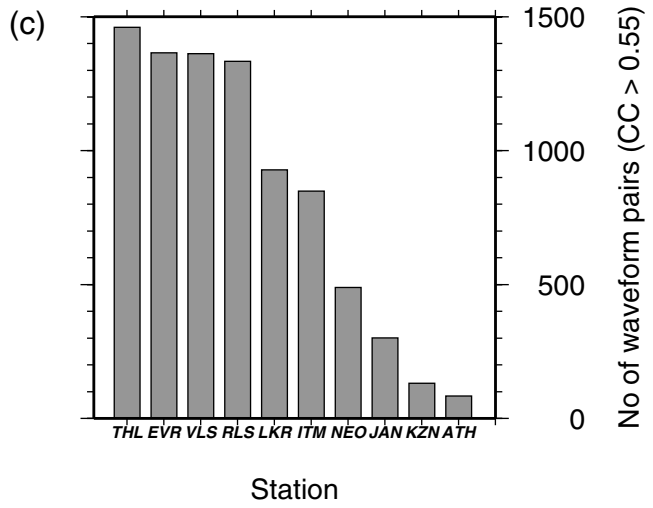

Figure 3. (a) Number of event pairs at different CC for *P* and *S* picks, respectively. (b) Number of event pairs with CC higher than 0.55 at different number of stations. (c) Number of waveform pairs with CC higher than 0.55 at stations used in the waveform relocation (see Fig. 1b for station locations).

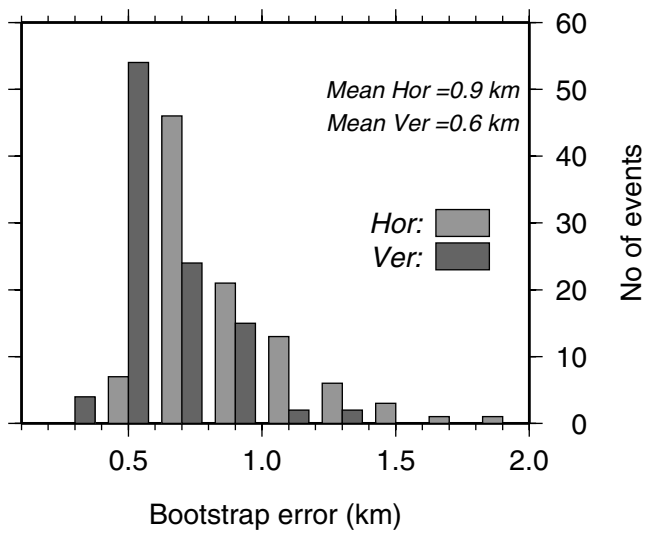

Figure 4. Horizontal and vertical bootstrap error in 0.2-km bins for the events relocated with waveform cross correlation. The mean values are also indicated.

ison between Figure 2b,c and Figure 4 shows that the location error estimates were significantly reduced after the SSST and WCC relocation. Figure 5 shows the locations of 101 events that were finally relocated using the procedure described previously, utilizing both the observed and differential travel times (Ⓔ see Table 1 in the electronic edition of *BSSA*).

Moment Tensor Inversion

We apply a linear, time-domain moment tensor inversion method with a point-source approximation (Randall *et al.*, 1995) in order to model the waveform data of the largest events of the swarm. Green's functions are calculated using the reflection method of Kennett (1983) as implemented by Randall (1994) and using the same 1D velocity model of Haslinger *et al.* (1999) that was utilized for the earthquake locations. Data preparation prior to inversion includes the reduction of velocity waveforms to displacement and rotation of the horizontal components into radial and transverse. The rotation is performed with respect to the epicenter stemming from the relocation procedure described previously. Both the data and the Green's functions are band-pass filtered between 0.05–0.08 Hz using a two-pole Butterworth filter and aligned according to their arrival times.

The waveforms are inverted assuming a vanishing isotropic component and a delta source time function. Inversions were repeated initially using a coarse depth interval of 5 km, followed by a finer one every 2 km around the depth that exhibited the minimum misfit. The criteria for including a station in the inversion process were (a) its azimuth relative to the epicenter so that different parts of the focal sphere could be covered, and (b) its epicentral distance, which should not exceed 150 km so that the source-receiver structure could be successfully approximated by our simple 1D

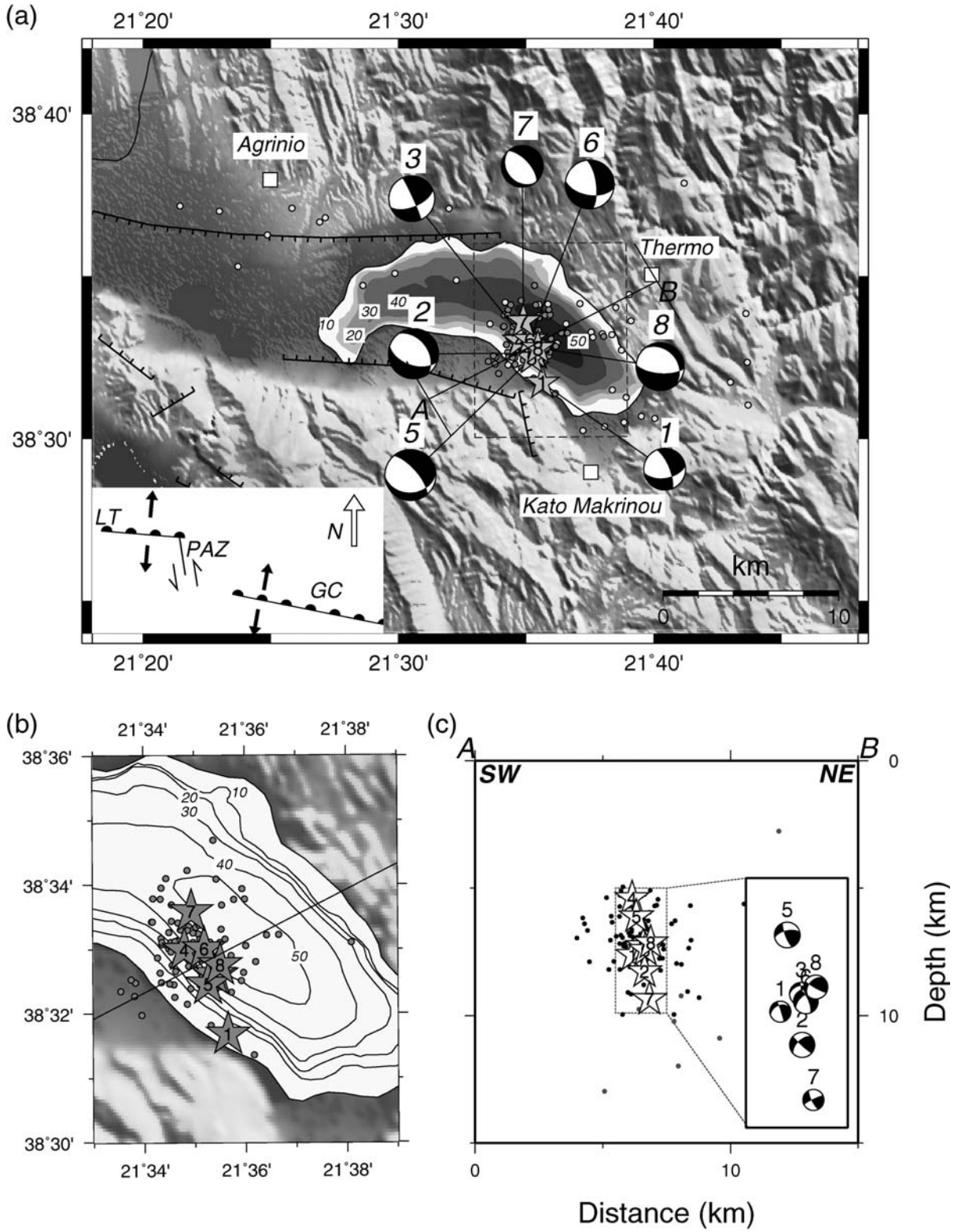

Figure 5. (a) Final relocation map of April–June 2007 Trichonis Lake earthquakes. Gray dots indicate events relocated with SSST and WCC methods, whereas white dots indicate events relocated with the SSST method only. Numbered stars mark the WCC relocations of the eight larger events and their focal mechanisms. Inside sketch demonstrates the stress regime in the region with Trichonis Lake, LT; Gulf of Corinth, GC; present studied activity zone, PAZ. Topographic relief, mapped faults, and nearby towns are also visible. Dashed rectangle marks a more detailed close up of the WCC-relocated events as shown in (b). (c) Cross-section AB marked in (a) that incorporates all relocated events within 5 km of the cross-section line. Focal mechanisms of seven out of the eight largest events are shown in the close-up cross section on the right. Focal spheres are lower hemispheres in map view and behind vertical plane hemispheres in the cross section.

velocity model. This analysis was applied to the seven largest events of the Trichonis swarm but not to the event on 10 April (07:14:13, M_L 4.2) because its waveforms were corrupted by the coda of the immediately previous event at 07:13:02. A summary of the source parameters for these events, as well as moment tensor inversion results, can be seen in Ⓔ Table 2 in the electronic edition of *BSSA*. We evaluate the quality of these solutions by jointly considering their average misfit (quality range A–D with A indicating misfit smaller than 0.3 and D larger than 0.7) and compensated linear vector dipole (CLVD) amount (quality range 1–4, with 1 indicating CLVD smaller than 20% and 4 indicating larger than 80%) (Ⓔ see also Table 3 in the electronic edition of *BSSA*). Based on these criteria, solutions 1–5 with qualities A1–B1 appear to be the most well constrained and indicate normal faulting with a substantial left-lateral strike-slip component (Fig. 5a).

Discussion

After the relocation using WCC, the event locations collapse in a north-northwest–south-southeast-trending cluster with a total length of ~6-km and ~3-km width lying on the offshore extension of the north-northwest–east-southeast fault that is mapped to the south of the lake (Fig. 5a). The relocated epicenters of the seven largest events in April 2007 (Fig. 5b, events 1–7) appear to have propagated in time from south-southeast to north-northwest direction, whereas the last event that occurred in June is located at the center of the cluster (Fig. 5b, event 8). A vertical cross section normal to the relocated alignment shows a near-vertical cluster at around 5–10-km depth dipping towards the northeast (Fig. 5c). Scattered epicenters that lie outside the major clusters are only located with the SSST method, and they are not considered as accurate. However, most of them lie eastwards of the north-northwest–south-southeast well-located alignment. The cluster geometry obtained agrees well with the best-constrained moment tensor solutions and furthermore helps in distinguishing the fault plane as the one dipping towards the northeast.

It is interesting to point out that the bathymetry of the lake exhibits an abrupt depth change along its southeast shore, and it quickly reaches the near-maximum depth towards the northeast direction. Our relocation results suggest that most of the events that occurred during the swarm originated beneath this part of the lake and at the extension of the onshore fault. This indicates, that the earthquake swarm under study could have been caused by the failure of a preexisting fault beneath the lake that had not been identified previously. Based on these results and the locations of the three largest events during the 1975 swarm activity (Fig. 1c) it is probable that the onshore section of the same fault might have been activated then. Despite the fact that the locations of these past events are not considered very accurate, this conclusion is supported by two other observations: (a) macroseismic intensity maps for these events (NOA-IG, 1975) show a similar pattern with an approximate northwest–southeast direction of the main contours and peak intensity VII+ at the village of Kato Makrinou, (b) an SR-100 Willmot seismoscope deployed at the nearby town of Messolongi showed deflections in a N120°E to N130°E direction for these events, indicating that the back azimuth of the incoming waves was to the southeast of Trichonis Lake.

Trichonis Lake is bounded by an almost west-northwest–east-southeast striking normal fault that lies close to the south shore and is marked by a major escarpment. It is also believed to be the youngest western extension of the Gulf of Corinth rift system (Brooks *et al.*, 1988; Melis *et al.* 1989). Oblique trending faults, like the one defined in our study, are linking the major west-northwest–east-southeast extensional structures that form the central Greece rift system and exhibit strike-slip components under the prevailing north–south extensional regime of the region. In particular, the north-northwest–south-southeast zone that has been identified in this study may form part of the eastward continuation link, connecting the major west-northwest–east-southeast Trichonis graben fault zone to the Gulf of Corinth rift system. Its oblique orientation with respect to the dominant north–south extensional stress field implies that some part of the deformation should be accommodated by left-lateral strike-slip motion, as it is actually observed in most of the moment tensor solutions (Fig. 5a, sketch). Finally, it must be mentioned that this suggested link cannot be seen at surface to continue towards the south due to the thick Hellenides thrust sequences. However, its existence has been suggested by the numerous swarms and moderate earthquakes that take place in the area and have also been recorded by temporary microearthquake surveys (Brooks *et al.*, 1988; Melis, 1992; Melis *et al.*, 1995).

Acknowledgments

The GMT mapping software (Wessel and Smith, 1995) was used for the preparation of the figures of this article. Topography and bathymetry in figures is extracted from topography maps of the Hellenic Military Geographical Service. Geological and fault information are taken from the Greek Institute of Geology and Mineral Explorations (IGME). NSM was partially supported by the GSRT-5189-Spain-2004-e-science Bilateral Agreement Grant and the NATO Collaborative Linkage Grant Number 979849. KIK was supported by the National Science Council of Taiwan. Thanks are due to Kuo-Fong Ma for useful discussions. Last but not least, we thank Keith Richards-Dinger and Diane Doser for their constructive comments that improved the initial manuscript.

References

Billings, S. D., M. S. Sambridge, and B. L. N. Kennett (1994). Errors in hypocenter location: picking, model, and magnitude dependence, *Bull. Seismol. Soc. Am.* **84,** 1978–1990.

Brooks, M., J. E. Clews, N. S. Melis, and J. R. Underhill (1988). Structural development of Neogene basins in western Greece, *Basin Res.* **1,** 129–138.

Doutsos, T., and S. Kokkalas (2001). Stress and deformation patterns in the Aegean region, *J. Struct. Geol.* **23,** 455–472.

Doutsos, T., N. Kontopoulos, and D. Frydas (1987). Neotectonic evolution of northwestern-continental Greece, *Geol. Rundsch.* **76,** 433–450.

Drakopoulos, J., and N. Delibasis (1982). Tech. Rept., The focal mechanism of earthquakes in the major area of Greece for the period of 1947–1981, University of Athens, Seismological Laboratory, Athens, Greece.

Goldsworthy, M., J. Jackson, and J. Haines (2002). The continuity of active fault systems in Greece, *Geophys. J. Int.* **148,** 596–618.

Haslinger, F., E. Kissling, J. Ansorge, D. Hatzfeld, E. Papadimitriou, V. Karakostas, K. Makropoulos, H. G. Kahle, and Y. Peter (1999). 3D crustal structure from local earthquake tomography around the Gulf of Arta (Ionian region, NW Greece), *Tectonophysics* **304,** 201–218.

Kennett, B. N. L. (1983). *Seismic Wave Propagation in Stratified Media*, Cambridge U Press, New York.

Klein, F. (2002). User's guide to HYPOINVERSE-2000, a Fortran program to solve for earthquake locations and magnitudes, *U.S. Geol. Surv. Open-File Rept. 02-171*.

Lin, G., and P. M. Shearer (2005). Tests of relative earthquake location techniques using synthetic data, *J. Geophys. Res.* **110,** B04304, doi 10.1029/2004JB003380.

Melis, N. (1992). Earthquake hazard and crustal deformation in central Greece, *Ph.D. Thesis*, Department of Geology, Cardiff University.

Melis, N. S., and K. I. Konstantinou (2006). Real-time seismic monitoring in the Greek region: an example from the 17 October 2005 East Aegean Sea earthquake sequence, *Seism. Res. Lett.* **77,** 364–370.

Melis, N. S., M. Brooks, and R. G. Pearce (1989). A microearthquake study in the Gulf of Patras region, western Greece, and its seismotectonic interpretation, *Geophys. J. Int.* **98,** 515–523.

Melis, N. S., P. W. Burton, and M. Brooks (1995). Coseismic crustal deformation from microseismicity in the Patras area, western Greece, *Geophys. J. Int.* **122,** 815–836.

NOA-IG (1975). Monthly bulletin, National Observatory of Athens, Institute of Geodynamics.

Papazachos, B., and K. Papazachou (1997). *The Earthquakes of Greece*, Ziti Editions, Thessaloniki, Greece.

Randall, G. E. (1994). Efficient calculation of complete differential seismograms for laterally homogeneous earth models, *Geophys. J. Int.* **118,** 245–254.

Randall, G. E., C. J. Ammon, and T. J. Owens (1995). Moment tensor estimation using regional seismograms from a Tibetan plateau portable network deployment, *Geophys. Res. Lett.* **22,** 1665–1668.

Richards-Dinger, K. B., and P. M. Shearer (2000). Earthquake locations in southern California obtained using source-specific station terms, *J. Geophys. Res.* **105,** 10,939–10,960.

Shearer, P. M. (1997). Improving local earthquake locations using the L1 norm and waveform cross correlation: application to the Whittier Narrows, California, aftershock sequence, *J. Geophys. Res.* **102,** 8269–8283.

Shearer, P. M., J. L. Hardebeck, L. Astiz, and K. B. Richards-Dinger (2003). Analysis of similar event clusters in aftershocks of the 1994 Northridge, California, earthquake, *J. Geophys. Res.* **108,** 2035, doi 10.1029/2001JB000685.

Shearer, P. M., E. Hauksson, and G. Q. Lin (2005). Southern California hypocenter relocation with waveform cross-correlation, part 2: Results using source-specific station terms and cluster analysis, *Bull. Seismol. Soc. Am.* **95,** 904–915.

Wessel, P., and W. H. F. Smith (1995). New version of the Generic Mapping Tools released, *EOS* **76,** 329.

Institute of Geodynamics
National Observatory of Athens
P.O. Box 20048
11810 Athens, Greece
cevan@gein.noa.gr
(C.P.E., N.S.M., M.C., G.N.S.)

Institute of Geophysics
National Central University
300 Jhongda Road
Taoyuan County, 320 Taiwan
(K.I.K.)

Manuscript received 18 July 2007